Formation of transverse cracks from the growth of multiple adjacent debonds on consecutive fibers in UD composites under transverse tension: Effect of the mutual position of debonds on Energy Release Rate

Luca Di Stasio · Janis Varna · Zoubir Ayadi

Abstract Models of Repeating Unit Cell (RUC) are developed to represent different Representative Volume Elements (RVEs) of UD composites of infinite size. Several damage states are studied in the form of different geometrical configurations of partially debonded and fully bonded fibers. It is found that the energetically most favorable cases for fiber/matrix interface crack (debond) growth are those where debonds grow on vertically (i.e. along thickness direction) aligned fibers. A maximum of Energy Release Rate (ERR) magnification is found when the vertically aligned partially debonded fibers are also contiguous.

1 Introduction

The process of damage onset and development in multi-axial Fiber Reinforced Polymer Composite (FRPC) laminates involves several fracture mechanisms, which concur to the final failure of the composite part. Upon loading, one of the first macroscopic mode of damage is the occurrence in transverse cracks in plies where fibers are not aligned with the remote applied loading. A single

Luca Di Stasio
Luleå University of Technology, University Campus, SE-97187 Luleå, Sweden
Université de Lorraine, EEIGM, IJL, 6 Rue Bastien Lepage, F-54010 Nancy, France
E-mail: luca.di.stasio@ltu.se

Janis Varna
Luleå University of Technology, University Campus, SE-97187 Luleå, Sweden
E-mail: janis.varna@ltu.se

Zoubir Ayadi
Université de Lorraine, EEIGM, IJL, 6 Rue Bastien Lepage, F-54010 Nancy, France
E-mail: zoubir.ayadi@univ-lorraine.fr

transverse crack does not significantly compromise the load-carrying of the laminate, but in large numbers transverse cracks become detrimental to the elastic response of the part under loading. Furthermore, high concentrantions of transverse cracks lead to stress re-distribution and stress concentrations that can promote other more dangerous mode of fracture, quickly leading to the global failure of the laminate or part. Understanding the factors that influence transverse cracks onset and propagation is thus fundamental to improve current laminate design and to identify mechanisms of controlled propagation, delay and suppression of transverse cracks. This would provide toughness to FRPC laminates and help to avoid early part replacement, and thus waste, currently in use to prevent sudden catastrophic brittle failure.

Early microscopic observations in glass fiber-epoxy cross-ply laminates determined that onset of transverse cracking occurs at the microscopic level in the form of fiber-matrix interface cracks (or debonds) [1]. Debonds grow along the arc direction of the fiber until reaching a critical size, then kink out of the interface and coalesce with other debonds across the ply thickness [24]. Once a through-the-thickness crack tunnels through the width of the laminate, a transverse crack is formed. Formation and growth of debonds at the microscale thus play a key role in the overall process of initiation of transverse cracking. To improve our understanding of the latter, the former must be studied and modeled.

The first investigations on the mechanics of fiber/matrix debonding proposed analytical models of a single partially debonded fiber placed in an infinite matrix. These models focused on understanding the effect of the elastic properties mismatch between fiber and matrix. They were firstly solved by Perlman and Sih [16], who provided the solution in terms of stress and displacement fields, and Toya [20], who evaluated the Energy Release Rate (ERR) at the debond tip. A closed-form analytical solution could only be found for the *open crack* case, which assumes that no contact between debond faces occurs. This solution was shown to provide, for large debonds, a non-physical solution that implies inter-penetration of crack faces [20,2]. Numerical treatment of the problem soon followed, in particular with the Boundary Element Method (BEM) solution by Paris et al. [14]. The numerical analysis of the single fiber model allowed first to understand the importance of crack face contact in the mechanics of fiber/matrix debonding [22], confirming earlier results regarding the straight bi-material interface crack [2]. The process of fiber/matrix debonding was investigated in models of a single partially debonded fiber embedded in an effectively infinite matrix under remote tension [14] and remote compression [3]. Residual thermal stresses were also analyzed [4]. The effect of a second nearby fiber was studied, under different uniaxial and biaxial tensile and compressive applied loads [5,6,17,18]. Debond growth in a hexagonal cluster of fibers embedded in an effectively homogenized UD composite was investigated by Zhuang et al. [25]. The interaction of two debonds facing each other on two nearby fibers was addressed in [23] for a cluster of fibers immersed in a homogenized UD.

Models of kinking were developed for a single fiber in an infinite matrix [15]

and a partially debonded fiber in a cluster of fibers inside a homogenized UD [26]. A study on linking of debonds was proposed in [23].

An analysis of the configuration preceding kinking and linking thus seems to lacking in the literature. We devote our attention in this paper to the analysis of Representative Volume Elements (RVEs) which model the presence of muliple debonds on fibers aligned across the thickness of UD composites. We focus on understanding the effect of the mutual interaction of consecutive debonds in the vertical direction and of their relative position, i.e. on the same or opposite sides of their respective fibers. We are interested in identifying which mechanisms might favor debond growth and which might, on the other hand, prevent it. For this reason, we select a regular arrangement of fibers and we adopt the approach of Linear Elastic Fracture Mechanics (LEFM) to characterize debond growth, by evaluating Mode I and Mode II Energy Release Rate (ERR). The Finite Element Method (FEM) is chosen to compute stress, strain and displacement fields, which are required to estimate ERR. The characteristics of the RVEs and the Finite Element (FE) solution are described in Sec. 2; the main results are reported and discussed in Sec. 3 and the main conclusions presented in Sec. 4.

2 RVE models & FE discretization

2.1 Introduction, properties and nomenclature

We focus in this article on debond growth in unidirectional (UD) composites subjected to in-plane transverse tensile loading. In particular, the interaction between debonds is studied through the development of models of Representative Volume Elements (RVE) of laminates with different configurations of debonds (see Fig. 1 and Fig. 2).

In order to facilitate the description of the models, let us assume that the UD composite mid-plane lies in the $x-y$ plane, where y coincides with the UD 0° direction while the $x-axis$ represents the UD in-plane transverse direction. Axis z is the through-the-thickness direction of the composite.

The composite RVE is defined in the $x-z$ plane and is repeating both along x and z. Mathematically, it corresponds to an infinite UD composite which models, practically, the behavior of debonds located far away from the laminate free surfaces. i.e. close to the laminate mid-plane, in a relatively thick UD composite (thickness > 100 fiber diameters). The composite with debonds is modeled as a sequence of fiber rows with or without debonds stacked on each other in the vertical (through-the-thickness) direction. Notice that each row contains only one fiber in the vertical direction. A regular microstructure is adopted for all RVEs, with fibers organized in a square-packing configuration. This choice is motivated by our interest in investigating the mechanisms that favors or prevent debond growth, and not in simulating crack path evolution in an arbitrary, randomized distribution of fibers. The regularity of the square-packing arrangement allows the identification of the different mecha-

Fig. 1: Representative Volume Element $n \times k - symm$ of a UD composite with debonds appearing after $n-1$ and after $k-1$ undamaged fibers respectively in the horizontal and vertical direction. In the vertical direction, on fibers belonging to the same "column", debonds are located always on the same side.

nisms influencing debond growth. Given their square-packing arrangement of fibers, each RVE is built by using the unit cell in Figure 3 as the basic building block. The unit cell contains one fiber place in its center and has a size of $2L \times 2L$, where

$$L = \frac{R_f}{2}\sqrt{\frac{\pi}{V_f}}. \tag{1}$$

In Equation 1, V_f is the fiber volume fraction and R_f the fiber radius. The fiber volume fraction is assumed equal to 60% in each RVE and the fiber radius equal to $1\mu m$. The choice of the previous value is not dictated

Fig. 2: Representative Volume Element $n \times k - asymm$ of a UD composite with debonds appearing after $n-1$ and after $k-1$ undamaged fibers respectively in the horizontal and vertical direction. In the vertical direction, on fibers belonging to the same "column", debonds are located on the opposite sides of consecutive fibers.

by physical considerations but by simplicity. It is thus useful to remark here that, in a linear elastic solution as the one considered in the present work, the ERR is proportional to the geometrical dimensions of the model and, consequently, recalculation of the ERR for fibers of any size requires a simple multiplication. Notice also that, given the relationship in Eq. 1 and that the unit cell is identically repeated following a square-packing configuration, V_f is homogeneous, i.e. no clustering of fibers is considered.

A glass fiber-epoxy UD composite is treated in the present work, and it is assumed that the response of each phase lies always in the linear elastic domain. The material properties of glass fiber and epoxy are reported in Table 1.
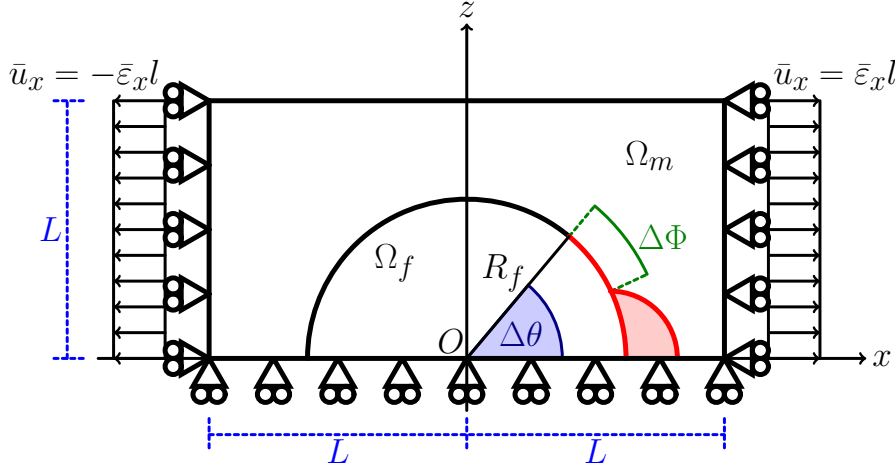
Fig. 3: Schematic of the model with its main parameters.

Table 1: Summary of the mechanical properties of fiber and matrix. E stands for Young's modulus, μ for shear modulus and ν for Poisson's ratio.

Material	$E\,[GPa]$	$\mu\,[GPa]$	$\nu\,[-]$
Glass fiber	70.0	29.2	0.2
Epoxy	3.5	1.25	0.4

We consider that upon application of a load in the x-direction, the strain response in the y-direction is small due to the very small minor Poisson's ratio of the UD composite. We also assume that debond size to be significantly larger in the fiber longitudinal direction than in the arc direction. We therefore use 2D models under the assumption of plane strain defined in the $x-z$ section of the composite, which allows us to focus our interest on debond growth along the arc direction. Assumptions of generalized plane strain would be more suited to represent the physics, however it would limit the scope of comparisons with previous studies in the literature. It is for this reason that plane strain conditions are preferred.

All RVEs are symmetric with respect to the horizontal direction, thus only half of the RVE is explicitly modeled and symmetry conditions are applied to the lower boundary of the RVE (Fig. 1 and Fig. 2). The number n of fibers in the horizontal directions and k in the vertical direction belonging to the RVEdetermine the total size of the RVE, described by its total length l and total height h:

$$l = n2L \qquad h = k2L;\qquad\qquad (2)$$

where $2L$ is the side length of the square unit cell previously introduced and L is defined according to Eq. 1. The number of fibers in the horizontal and vertical directions determine as well the damage state of the modeled UD

composite. In particular, a $n \times k$ RVE represents a UD composite in which a debond appear after $n - 1$ fully bonded fibers inside a fiber row, and a fiber row contains debonds after $k - 1$ fiber rows with no damage (see Fig. 1 and Fig. 2). To model such configurations, conditions of coupling of the horizontal displacement u_x are applied to the right and left boundary, which ensures that the computed solution represents a model in which the RVE is repeated infinite times in the horizontal direction. It is worth to highlight that the repetition of the RVE occurs in a mirror-like fashion: moving along the x-axis, if a debond appears on the right side of its fiber, the next one is placed on the left side.

This might lead to extreme conditions in the model. Consider for example the case of $1 \times k$ RVEs: inside a fiber row containing damage, an infinite number of debonds is present and debonds are facing each other pair-by-pair. Such configuration is physically unlikely, however the evaluation of the ERR in this case provides a bound for the case of maximum debond mutual interaction in the vertical direction. Thus, the models proposed here might represent extreme configuration, but they provide theoretical bounds for debond behavior in an actual composite. In particular, observations regarding mechanisms favoring debond growth will represent an upper bound on ERR and thus a conservative estimation of the actual behavior, still of use for the structural designer. Greater care should instead be taken when considering mechanisms preventing debond growth: the ERR estimate provided by our models would be a lower bound, thus debond growth might be higher than predicted in the actual composite.

Repetition occurs also along the vertical direction. Here two cases can be distinguished: first, debonds aligned in the vertical direction are placed on the same side of their respective fibers as in Figure 1; second; debonds aligned in the vertical direction are placed on alternating opposite sides of their respective fibers in Figure 2. The first is case of symmetric repetition with respect to the upper boundary of the RVE; the second case is one of anti-symmetric repetition with respect to the upper boundary of the RVE. The two different families of RVEs (symmetric with respect to anti-symmetric repetition) are thus respectively called $n \times k - symm$ and $n \times k - asymm$. The details of the boundary conditions adopted in the two different cases are described in Sec. 2.2.

2.2 Equivalent boundary conditions: description and validation

Two main families of Representative Volume Elements have been introduced in the previous section, distinguished by their pattern of repetition along the vertial direction: $n \times k - symm$ and $n \times k - asymm$.

To model the symmetric repetition of $n \times k - symm$ RVE (Fig. 1) we adopt,

on the upper boundary, conditions of coupling of the vertical displacements u_z of the type

$$u_z(x, h) = \bar{u}_z, \tag{3}$$

where h is the total height of the RVE defined in Eq. 2 and $\bar{u}_z$ is the constant value of the vertical displacement, equal for all the points on the upper boundary. The value of $\bar{u}_z$ is *a priori* unknown and is evaluated as part of the elastic solution.

The asymmetric repetition of $n \times k - asymm$ RVE (Fig. 2) is modeled with the following set of conditions applied to the vertical u_z and horizontal displacements u_x:

$$u_z(x, h) - u_z(0, h) = -(u_z(-x, h) - u_z(0, h))$$
$$u_x(x, h) = -u_x(-x, h), \tag{4}$$

where h is again the total height of the RVE and $u_z(0, h)$ is the vertical displacement of the upper boundary mid-point, which is always located at coordinates $(0, h)$. Similarly to $\bar{u}_z$ in the symmetric case, $u_z(0, h)$ is *a priori* unknown and is computed as part of the elastic solution.
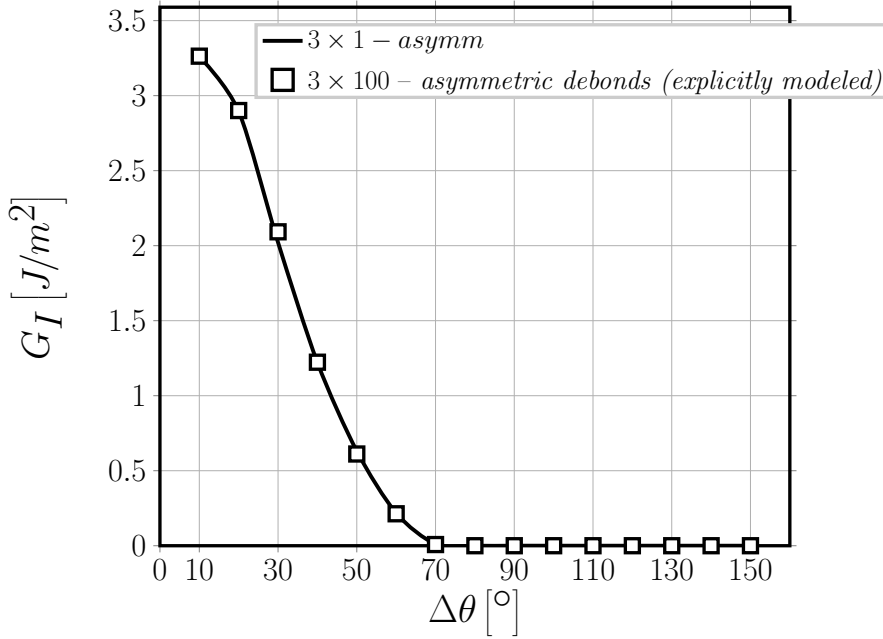

Fig. 4: Validation of asymmetric coupling conditions of Eq. 4: Mode I ERR, $V_f = 60\%$, $\bar{\varepsilon}_x = 1\%$.

To the authors' knowledge, this is the first time the set of boundary conditions of Eq. 4 is proposed and used to model an asymmetric coupling as the one reported in Figure 2. To validate them, Mode I (Fig. 4) and Mode II ERR (Fig. 5) are evaluated for $3 \times 1 - asymm$ RVE and compared with the results of the $3 \times 100 - asymmetric\ debonds$ (*explicitly modeled*) RVE, in the case of an applied strain $\bar{\varepsilon}_x$ of 1%. The $3 \times 201 - asymmetric\ debonds$ (*explicitly modeled*) RVE possesses, as all other RVEs studied here, conditions of coupling of the horizontal displacement applied to the left and right side. It is as well symmetric with respect to the x-axis, thus only half of the RVE is modeled and conditions of symmetry are applied to the lower horizontal boundary. The upper side of the RVE is, differently from the other models studied here, left free. Debonds are explicitly modeled and placed on alternating sides of vertically aligned fibers, i.e. if a fiber has a debond on the right side the next fiber above will have the debond on the left side. Debonds are all of the same size. The $3 \times 201 - asymmetric\ debonds$ (*explicitly modeled*) RVE thus represents the same configuration as the $3 \times 1 - asymm$ RVE, but explicitly modeled. Comparison of the ERR of the two RVEs provides a validation of accuracy of the conditions expressed in Eq. 4 as a mean to represent the situation with alternating debonds (or asymmetric coupling, as depicted in Fig. 2 with the use of equivalent boundary conditions, which is a more effective in terms of computational cost of the model (time and memory needed to compute the solution).

As shown in Figure 4 and Figure 5, a very good agreement is obtained between the results of the two RVEs for both Mode I and Mode II ERR. The validity of the asymmetric coupling conditions proposed in Equation 4 is thus confirmed.

2.3 Finite Element (FE) solution

The solution of the elastic problem is obtained with the Finite Element Method (FEM) within the Abaqus environment, a commercial FEM software [19].
The debond is placed symmetrically with respect to the x axis (see Fig. 3) and it is characterized by an angular size of $\Delta\theta$ (making the full debond size equal to $2\Delta\theta$). For large debond sizes (at least $\geq 60° - 80°$), a region $\Delta\Phi$ of variable size appears at the crack tip where the crack faces are in contact but free to slide relatively to each other. In order to model crack faces motion in the contact zone, frictionless contact is considered between the two crack faces to allow free sliding and avoid interpenetration.
A constant displacement is applied to all RVEs, the magnitude of which is selected to have a constant applied horizontal strain $\bar{\varepsilon}_x$ equal to 1%. The choice of this specific value of the applied strain is actually arbitrary. In the context of Linear Elastic Fracture Mechanics, the Energy Release Rate at the debond tip is proportional to the square of the applied strain. Thus, ERR estimation at a different strain level requires a simple multiplication. Furthermore, our interest is to compare the effect of different mechanisms on debond growth,
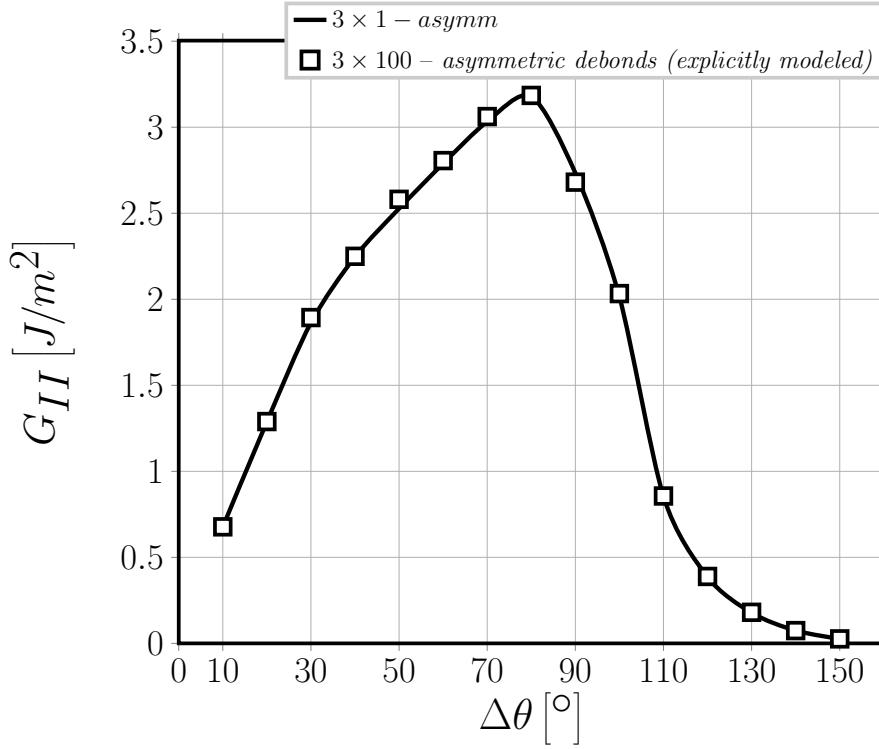
Fig. 5: Validation of asymmetric coupling conditions of Eq. 4: Mode II ERR, $V_f = 60\%$, $\bar{\varepsilon}_x = 1\%$.

which we characterize with Mode I and Mode II ERR. As such, our focus is not on providing absolute values of ERR for specific damage configurations, but rather to assess and compare the relative changes in ERR due to modifications of the sorrounding environment. In this perspective, the selection of a rather large value of the applied strain helps our understanding by magnifying the differences in ERR. A further consideration regarding the magnitude of the load needs to be made, regarding the presence of contact between debond faces. The problem solved is a linear problem with non-holonomic constraints due to the non-interpenetration conditions (inequalities) enforced on crack faces relative displacements. In particular, the problem falls under the definition of receding contact problem [14,9]. This family of problems in LEFM has some peculiar characteristics [9,11,21]: the size and shape of the contact zone does not depend on the magnitude of the applied load, but only on its type. Thus, upon a change in magnitude of the applied strain $\bar{\varepsilon}_x$ the size and shape of the contact zone at the fiber/matrix interface will remain the same.

Meshing of the model is accomplished with second order, 2D, plane strain triangular (CPE6, see [19]) and quadrilateral (CPE8, see [19]) elements. An oscillating singularity exists at the debond tip in the stress and displacement

fields [8, 20, 2]. The presence of this singularity prevents the convergence of Mode I and Mode II ERR at the debond tip. Thus, a correct Mode decomposition of the ERR can not be computed in the theoretical limit of an infinitesimal crack increment. It is possible however to avoid the issue by approximating the Mode decomposition over a finite instead of an infinitesimal crack increment. This leads naturally to the use of the Virtual Crack Closure Technique (VCCT) [12], which estimates Mode I and Mode II ERR over a finite crack increment corresponding to the size of the element at the crack tip. To obtain accurate results in terms of Mode decomposition of the ERR, care must be taken in ensuring the quality of the mesh at the debond tip. In particular, a regular mesh of 8-node (2nd order rectangular) elements with almost unitary aspect ratio is constructed at the debond tip. The angular size δ of an element in the debond tip neighborhood is always equal to $0.05°$. The crack faces are modeled as element-based surfaces and a small-sliding contact pair interaction with no friction is imposed between them. The Mode I, Mode II and total Energy Release Rates (ERRs) (respectively referred to as G_I, G_{II} and G_{TOT}) are the main result of FEM simulations; they are evaluated using the VCCT [12] implemented in a in-house Python routine. Validation is performed with respect to the results reported in [15, 17], which were obtained with the Boundary Element Method (BEM) for a model of a partially debonded single fiber placed in an infinite matrix. As discussed in more detail in [7], the agreement between FEM (present work) and BEM [15, 17] solutions is good and the difference between the two does not exceed 5%. This provides us with a level of uncertainty with which we can analyze the significance of observed trends: any relative difference in ERR between different RVEs smaller than 5% cannot be reliably distinguished from numerical uncertainty and its discussion should thus be avoided.

3 Results & Discussion

3.1 Effect of debonds mutual position and presence of fiber columns with no damage on the growth of multiple adjacent debonds along the vertical direction

We first focus our attention on comparing $n \times 1 - symm$ and $n \times 1 - asymm$ RVEs, with $n = 3, 11, 101, 201$. Both RVEs model a UD composite in which debonds appear on consecutive fibers aligned in the vertical direction, i.e. a "column" of fibers or, in the following, simply a fiber column. In $n \times 1 - symm$ and $n \times 1 - asymm$ a fiber column containing only partially debonded fibers is present after $n - 1$ fiber columns with no damage. Two main effects on debond ERR are analyzed through the comparison of these two families of RVEs: for a given type of RVE ($n \times 1 - symm$ vs $n \times 1 - asymm$), the effect of an increasing number of fiber columns with no damage between fiber columns containing damage; for a given number n fiber columns with no damage present in the model, the effect of the mutual position of consecutive debonds, i.e. on

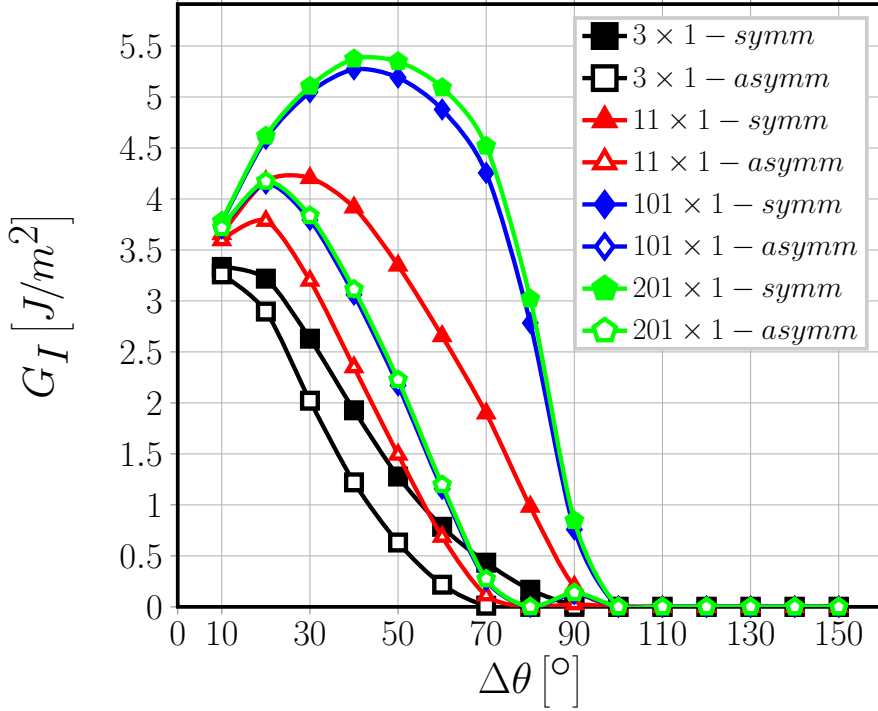the same side ($n \times 1 - symm$) or on opposite sides ($n \times 1 - asymm$) of their respective fiber.

Fig. 6: Effect of debonds mutual position on Mode I ERR: models $n \times 1 - symm$ and $n \times 1 - asymm$. $V_f = 60\%$, $\varepsilon_x = 1\%$.

By looking at Figure 6 and Figure 7, it is possible to conclude that, for both $n \times 1 - symm$ and $n \times 1 - asymm$ RVEs, increasing the number of fiber columns with no damage between fiber columns containing damage causes an increase in both Mode I and Mode II ERR. A few, more specific, observations can be made. For Mode I ERR in Figure 6, increasing the number of fiber columns with no damage causes also a roughly $10°$ delay of the onset of the contact zone: from a debond size of $70°$ to $80°$ for $n \times 1 - asymm$ and from $\Delta\theta = 90°$ to $100°$ for $n \times 1 - symm$. The occurrence of the maximum value of G_I is also delayed: from $\Delta\theta = 10°$ to $20°$ for $n \times 1 - asymm$ and from $\Delta\theta = 10°$ to $40°$ for $n \times 1 - symm$. For Mode II ERR as well (Figure 6), the occurrence of the maximum value of G_{II} is delayed: from $80°$ to $100°$ for $n \times 1 - asymm$ and from $60°$ to $90°$ for $n \times 1 - symm$. Comparing on the other hand the ERR of $n \times 1 - symm$ and $n \times 1 - asymm$ RVEs for a given value of n, it is possible to observe that: for Mode I in Figure 6, the ERR is always higher for $n \times 1 - symm$, i.e. when debonds occur on the same side

of the damaged vertically-aligned fibers; for Mode II in Figure 7, the values
of ERR of the two RVEs remain indentical or very close to each other when
$\Delta\theta < 80°$, while for larger debonds $n \times 1 - asymm$ presents the higher values
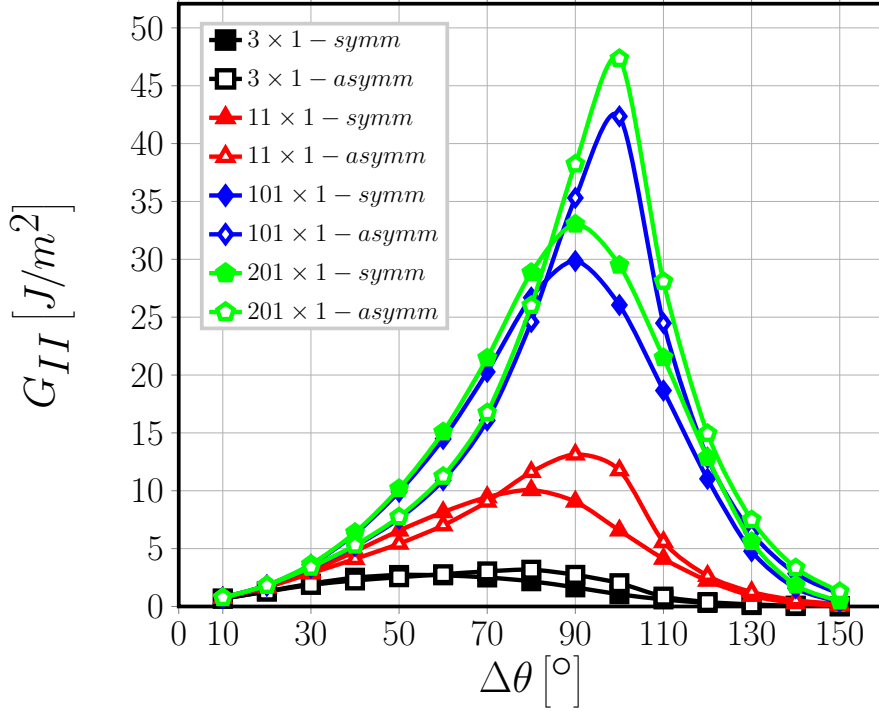of ERR.

Fig. 7: Effect of debonds mutual position on Mode II ERR: models $n \times 1 - symm$
and $n \times 1 - asymm$. $V_f = 60\%$, $\varepsilon_x = 1\%$.

The increase in Energy Release Rate due to an increasing number of fiber
columns with no damage between fiber columns containing debonds is a conse-
quence of the strain magnification effect. The addition of undamaged elements
(fiber columns with no damage) in the RVE causes an increase of the global
average strain in the material and thus an increase of strain and displacement
at the debond tip, to which the ERR is proportional. A look at this phe-
nomenon from the opposite point of view is helpful for understanding. From
the opposite perspective, Figure 6 and Figure 7 show that the ERR decreases
with an increasing number of fiber columns containing debonds. The presence
of cracks, in the form of debonds, in the composite causes discontinuities (or
jumps) in the strain and displacement field, which leads to a decrease in the
average global strain in the material. As the average global strain decreases,
the local values of strain and displacement at the debond tip decrease and thus

the Energy Release Rate decreases. The two perspectives are complementary to each other for the understanding of the results in Fig. 6 and Fig. 7.

In the context of Linear Elastic Fracture Mechanics, a critical Energy Release Rate is assumed to exist and to be a material property, independent of load and geometry. According to Griffith criterion, if the crack ERR is higher than the critical ERR, growth will occur. As a consequence, higher values of ERR could usually be taken as a proxy for the likelihood of crack growth: the configuration with the higher ERR would be the most likely to propagate. Thus, a simple comparison of relative magnitudes of ERR would tell which mechanism favors and which one prevents crack growth. However, the problem is more complex in the case of debonding at the fiber/matrix interface. Although the existence of a critical Energy Release Rate can be postulated, it has been found that its value actually depends on the Mode ratio at the debond tip [10]. The functional form of this dependence is still an open issue, although suggestions have been made [10,13]. A commonality of the different proposed criteria of critical ERR is that it is lower in pure Mode I and Mode I-dominated regimes and increases quickly with the increase in the Mode II contribution to the total ERR, reaching the highest value for pure Mode II behavior. It can be concluded that, in general, debonding will likely occur in pure Mode I or Mode I-dominated Energy Release Rate. Getting back to the results of our analysis, observation of Figure 6 implies that a symmetric placement of debonds along the vertical direction, i.e. debonds on the same side of their fibers, would favor the Mode I-dominated growth of small debonds ($\Delta\theta < 80° - 90°$) more than an asymmetric placement, i.e. debonds on opposite sides. From observation of Figure 7 we can instead conclude that: for large debonds ($\Delta\theta > 80° - 90°$) it is likelier that, for a given value of n, the ERR-based condition of propagation is satisfied in the case of an asymmetric placement of debonds along the vertical direction, given the higher value of Mode II ERR with the respect to $n \times 1 - symm$; provide that for a given value of n the ERR-based condition of propagation is satisfied, larger debond sizes would be obtained in the case of an asymmetric placement of debonds, given that the maximum Mode II ERR occurs at higher values of $\Delta\theta$ for $n \times 1 - asymm$ with respect to $n \times 1 - symm$.

3.2 Effect of the presence of undamaged fibers on debond-debond interaction along the vertical direction

It is at this point interesting to investigate the effect of the presence of undamaged (fully bonded) fibers between debonds along the vertical direction on debond-debond interaction. To this end, we study the $n \times 3 - symm$ and $n \times 3 - asymm$ RVEs, with $n = 3, 7, 21, 101$.

Results reported in Figure 8 and Figure 9 respectively for Mode I and Mode II show that the presence of only two undamaged fibers placed between debonds along the vertical direction makes the results of $n \times 3 - symm$ and $n \times 3 - asymm$ undistinguishable. It appears that the relative placement of
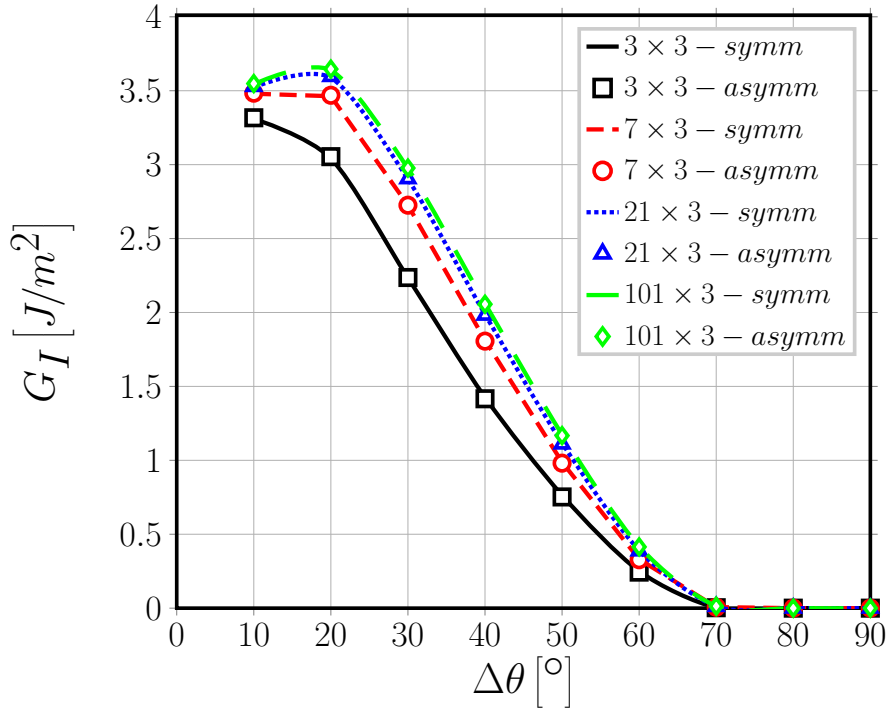
Fig. 8: Effect of the presence of undamaged fibers along the vertical direction on Mode I ERR: models $n \times 3 - symm$ and $n \times 3 - asymm$. $V_f = 60\%$, $\varepsilon_x = 1\%$.

debonds does not have any relevant effect on debond ERR, and thus on debond growth, when undamaged fibers are present in between.

Furthermore, comparison of Figure 6 with Figure 8 for Mode I and of Figure 7 with Figure 9 for Mode II shows that, especially for Mode II ERR, the presence of fully bonded fibers between debonds along the vertical direction reduces the strain magnification effect due to the presence of additional fiber columns with only fully bonded fibers along the horizontal direction. Mode I reaches a maximum of 5.5 J/m^2 for $101 \times 1 - symm$ and 4 J/m^2 for $101 \times 1 - asymm$ (Figure 6), and of 3.5 J/m^2 for both $101 \times 3 - symm$ and $101 \times 3 - asymm$ (Figure 8). The maximum value of Mode II is 30 J/m^2 for $101 \times 1 - symm$ and 42.5 J/m^2 for $101 \times 1 - asymm$ (Figure 7), and of 4.75 J/m^2 for both $101 \times 3 - symm$ and $101 \times 3 - asymm$ (Figure 9).

4 Conclusions

Different models of infinite UD composites have been studied with different configurations of multiple interacting debonds in order to investigate their effect of Mode I and Mode II Energy Release Rate.
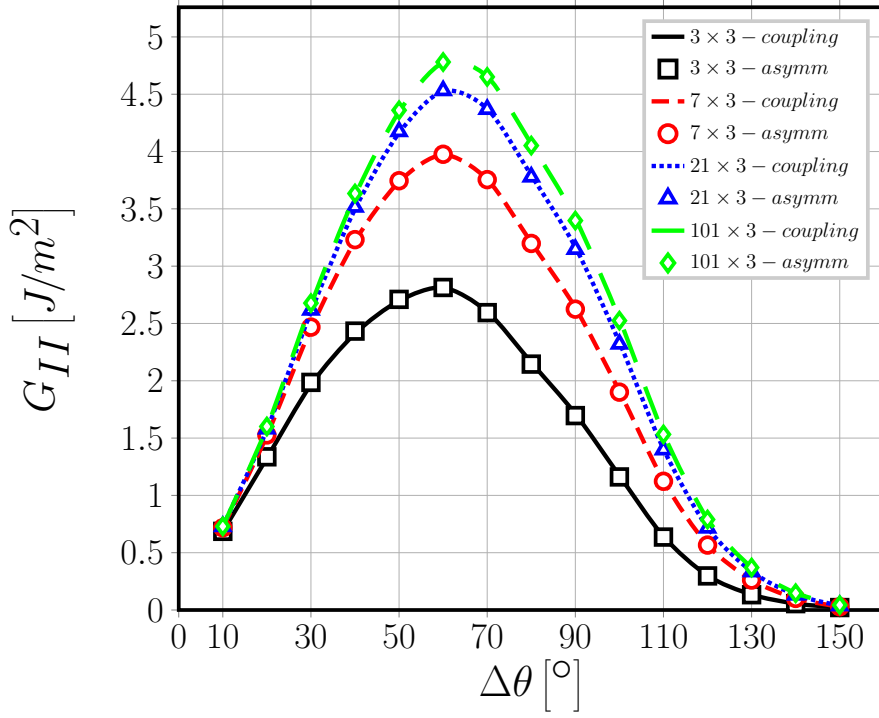
Fig. 9: Effect of the presence of undamaged fibers along the vertical direction on Mode II ERR: models $n \times 3 - symm$ and $n \times 3 - asymm$. $V_f = 60\%$, $\varepsilon_x = 1\%$.

Building upon the observations made in the previous section, several conclusions can be drawn about the growth of debonds in UD composites:

- at given strain level, multiple debonds can appear on not consecutive vertically-aligned fibers;
- at a given strain level, the vertical lines of fibers on which debonds grow are determined by the horizontal distance from pre-existing debonds;
- a minimum non-interactive distance exists for the Energy Release Rate;
- when spacing between vertical lines of debonds is lower than the minimum non-interactive distance, the ERR decreases;
- thus, conversely, when spacing between vertical lines of debonds is lower than the minimum non-interactive distance, higher levels of strain are needed to grow debonds;
- growth of debonds appearing on contiguous vertically-aligned fibers is energetically the most favorable;
- larger debonds are favored on contiguous vertically aligned partially debonded fibers.

References

1. Bailey, J.E., Parvizi, A.: On fibre debonding effects and the mechanism of transverse-ply failure in cross-ply laminates of glass fibre/thermoset composites. Journal of Materials Science **16**(3), 649–659 (1981). DOI 10.1007/bf02402782
2. Comninou, M.: The interface crack. Journal of Applied Mechanics **44**(4), 631 (1977). DOI 10.1115/1.3424148
3. Correa, E., Gamstedt, E., París, F., Mantič, V.: Effects of the presence of compression in transverse cyclic loading on fibre–matrix debonding in unidirectional composite plies. Composites Part A: Applied Science and Manufacturing **38**(11), 2260–2269 (2007). DOI 10.1016/j.compositesa.2006.11.002
4. Correa, E., Mantič, V., París, F.: Effect of thermal residual stresses on matrix failure under transverse tension at micromechanical level: A numerical and experimental analysis. Composites Science and Technology **71**(5), 622–629 (2011). DOI 10.1016/j.compscitech.2010.12.027
5. Correa, E., París, F., Mantič, V.: Effect of the presence of a secondary transverse load on the inter-fibre failure under tension. Engineering Fracture Mechanics **103**, 174–189 (2013). DOI 10.1016/j.engfracmech.2013.02.026
6. Correa, E., París, F., Mantič, V.: Effect of a secondary transverse load on the inter-fibre failure under compression. Composites Part B: Engineering **65**, 57–68 (2014). DOI 10.1016/j.compositesb.2014.01.005
7. Di Stasio, L., Varna, J., Ayadi, Z.: Energy release rate of the fiber/matrix interface crack in UD composites under transverse loading: effect of the fiber volume fraction and of the distance to the free surface and to non-adjacent debonds. Theoretical and Applied Fracture Mechanics p. 102251 (2019). DOI 10.1016/j.tafmec.2019.102251
8. England, A.: On stress singularities in linear elasticity. International Journal of Engineering Science **9**(6), 571–585 (1971). DOI 10.1016/0020-7225(71)90039-5
9. Garrido, J., Foces, A., Paris, F.: B.e.m. applied to receding contact problems with friction. Mathematical and Computer Modelling **15**(3-5), 143–153 (1991). DOI 10.1016/0895-7177(91)90060-k
10. Hutchinson, J., Suo, Z.: Mixed mode cracking in layered materials. In: Advances in Applied Mechanics, pp. 63–191. Elsevier (1991). DOI 10.1016/s0065-2156(08)70164-9
11. Keer, L.M., Dundurs, J., Tsai, K.C.: Problems involving a receding contact between a layer and a half space. Journal of Applied Mechanics **39**(4), 1115 (1972). DOI 10.1115/1.3422839
12. Krueger, R.: Virtual crack closure technique: History, approach, and applications. Applied Mechanics Reviews **57**(2), 109 (2004). DOI 10.1115/1.1595677
13. Mantič, V.: Interface crack onset at a circular cylindrical inclusion under a remote transverse tension. application of a coupled stress and energy criterion. International Journal of Solids and Structures **46**(6), 1287–1304 (2009). DOI 10.1016/j.ijsolstr.2008.10.036
14. París, F., Caño, J.C., Varna, J.: The fiber-matrix interface crack — a numerical analysis using boundary elements. International Journal of Fracture **82**(1), 11–29 (1996). DOI 10.1007/bf00017861
15. París, F., Correa, E., Mantič, V.: Kinking of transversal interface cracks between fiber and matrix. Journal of Applied Mechanics **74**(4), 703 (2007). DOI 10.1115/1.2711220
16. Perlman, A., Sih, G.: Elastostatic problems of curvilinear cracks in bonded dissimilar materials. International Journal of Engineering Science **5**(11), 845–867 (1967). DOI 10.1016/0020-7225(67)90009-2
17. Sandino, C., Correa, E., París, F.: Numerical analysis of the influence of a nearby fibre on the interface crack growth in composites under transverse tensile load. Engineering Fracture Mechanics **168**, 58–75 (2016). DOI 10.1016/j.engfracmech.2016.01.022

18. Sandino, C., Correa, E., París, F.: Interface crack growth under transverse compression: nearby fibre effect. In: Proceeding of the 18th European Conference on Composite Materials (ECCM-18) (2018)
19. Simulia, Providence, RI, USA: ABAQUS/Standard User's Manual, Version 6.12 (2012)
20. Toya, M.: A crack along the interface of a circular inclusion embedded in an infinite solid. Journal of the Mechanics and Physics of Solids **22**(5), 325–348 (1974). DOI 10.1016/0022-5096(74)90002-7
21. Tsai, K.C., Dundurs, J., Keer, L.M.: Elastic layer pressed against a half space. Journal of Applied Mechanics **41**(3), 703 (1974). DOI 10.1115/1.3423375
22. Varna, J., París, F., C.Caño, J.: The effect of crack-face contact on fiber/matrix debonding in transverse tensile loading. Composites Science and Technology **57**(5), 523–532 (1997). DOI 10.1016/s0266-3538(96)00175-3
23. Varna, J., Zhuang, L.Q., Pupurs, A., Ayadi, Z.: Growth and interaction of debonds in local clusters of fibers in unidirectional composites during transverse loading. Key Engineering Materials **754**, 63–66 (2017). DOI 10.4028/www.scientific.net/kem.754.63
24. Zhang, H., Ericson, M., Varna, J., Berglund, L.: Transverse single-fibre test for interfacial debonding in composites: 1. experimental observations. Composites Part A: Applied Science and Manufacturing **28**(4), 309–315 (1997). DOI 10.1016/s1359-835x(96)00123-6
25. Zhuang, L., Pupurs, A., Varna, J., Talreja, R., Ayadi, Z.: Effects of inter-fiber spacing on fiber-matrix debond crack growth in unidirectional composites under transverse loading. Composites Part A: Applied Science and Manufacturing **109**, 463–471 (2018). DOI 10.1016/j.compositesa.2018.03.031
26. Zhuang, L., Talreja, R., Varna, J.: Transverse crack formation in unidirectional composites by linking of fibre/matrix debond cracks. Composites Part A: Applied Science and Manufacturing **107**, 294–303 (2018). DOI 10.1016/j.compositesa.2018.01.013